Journal of Engineering Science and Technology
Vol. 9, No. 5 (2014) 657 - 669

EXPERIMENTAL AND NUMERICAL STUDY OF THE SWIRLING FLOW IN CONICAL DIFFUSERS

J.G. COELHO[1,*], R.Q. NEIVA[2], A.J. SOUSA[2], A.C.P. BRASIL JUNIOR[2]

[1]Federal University of Triângulo Mineiro, Department of Mechanical Engineering,
Avenida Doutor Randolfo Borges Junior, 1250 – Uberaba – MG, Brazil
[2]University of Brasilia, Department of Mechanical Engineering,
Campus Darcy Ribeiro, Brasilia – DF- Brazil
*Corresponding Author: josegustavo@icte.uftm.edu.br

Abstract

The aim of the present work is to analyse experimental and numerically the swirling turbulent flow in conical diffusers. The experimental part is made with Particle Image Velocimetry (PIV), where two geometries 5 and 10° semi-angles are analysed. We obtain information of the mean flow, in the axial and also in the cross sections of the swirling flow. In each PIV plane, two velocity components are obtained. Using the same conditions of the experimental apparatus, it is numerical simulation using CFX 14. We used Reynolds Averaged Navier-Stokes (RANS) for solve the closing problem and Shear Stress Transport (SST) turbulence modelling. In comparing the results, it was observed that the data had good quantitative agreement.

Keywords: PIV, RANS, Swirling flow, Turbulence.

1. Introduction

The diffusers are used to reduce the flow speed and to increase its static pressure, in other words, to convert kinetic energy in pressure energy. With this important characteristic the diffusers present several applications in different engineering branches, including hydroelectric turbines [1], combustors [2], rocketry [3], among many other applications.

Another subject that shows great interest, in the current days, is the analysis of swirling flows, generated by turbine rotors, guidelines blades in the hydraulic machines and combustors, and cyclones. There is in the literature countless works on those important themes, as the work accomplished by Hac [4], where calculations are

Nomenclatures

k	Turbulent kinetic energy, m^2/s^2
p	Pressure, Pa
$(S_{ij}S_{ij})^{1/2}$	Invariants of the stress deviation tensor, Pa
u_i	Velocity components, m/s
x_i	Spatial components, m
y	Distance of the sliding surface, m

Greek Symbols

θ	Semi-angle of the diffuser, deg.
ν_t	Eddy viscosity, Pa.s
ρ	Density, kg/m^3
τ_{ij}	Viscous stress tensor, Pa
ω	Specific Dissipation Rate, 1/s

made for different diffusers and the influence of the insertion of the swirl at the entrance of the diffuser is also evaluated. Azad [5] presents an analysis of diffuser flow, with emphasis in the aspects of turbulent flow. In this work the mean velocity profiles were obtained throughout the diffuser. Ishizaka et al. [6] presents a study using Computational Fluid Dynamics (CFD) in diffusers of gas turbines, where the performance of exhaust diffuser is improved in consideration of the distortion of the flow of the turbine exit.

Clausen et al. [7] evaluate the development of the swirl flow in the turbulent boundary layer of a conical diffuser. The geometry used was an conical diffuser with semi-angle10° included angle and an area ratio of 2.84, and the inlet swirl was close to solid-body rotation and was of sufficient magnitude to prevent boundary layer separation but just insufficient to cause recirculation in the core flow. Edwards et al. [8] compare two experimental techniques to quantify the swirl in the entrance of an annular diffuser. The authors used the liquid crystal technique that is an easy-to-use and attractive low-cost alternative to the more traditional approach.

Other works also deserve prominence, as accomplished by Japikse [9] that determines the correlation between the swirls geometry and the aerodynamic for the efficiency of an annular diffuser. In this study, a sensible baseline correlation has been established which is suitable for preliminary design of some turbine systems; Iaccarino [10], that compares the results obtained by different commercial solvers in the study of the turbulence in diffuser flows. Coelho et al. [11], made an expressive analysis of the influence of the swirl in the development of diffuser flow. He showed that depending on the swirl number the performance of the diffuser could be increased up to a limit point. From that point, the yield begins to decline and finally Coelho et al. [12] that accomplishes a transient study of the conical diffuser flows. This work shows that for certain angles are necessary to consider the transient part of the phenomenon.

In most of the cases where diffusers are used, it is important to evaluate the amount of pressure that the diffuser is able to recover. That is directly related with the stall of the boundary layer and recirculation produced in the central region of

the diffuser. Those factors are directly related to the income of the diffuser. It is considered the separation of the boundary layer being function of the conditions at the entrance of the diffuser, the exit conditions, the Reynolds number, the Mach number, and also on the geometry of the diffuser. According to Blevins [13], when the number of Reynolds is above 5×10^4, the flow separation becomes a function basically of the diffuser geometry. However, when a swirl is placed in the flow the situation will vary, because depending of the intensity of rotation (swirl number) can achieve good performance for the diffuser, even with a high total angle. If the rotation is small there will be a displacement of the boundary layer. If the rotation is large, recirculation will be present in the central part [11].

This work presents experimental and numerical flow results to obtain information of the mean flow, in the axial and also in the cross sections of the swirling flow. We use two different geometries, where the semi-angles are 5° and 10° (equivalent to total angles of the 10^o and 20°, respectively). The two geometries have the same area ratio and it is expected that there is separation from the wall since for semi-angles greater (or equal) to 5°, this phenomenon is observed [14].

For the numerical simulation it is used the CFX-14 of ANSYS package. This software is used for geometry creation and mesh generation, as well to impose the flow boundary conditions, processing and post processing. The Reynolds Averaged Navier-Stokes (RANS) modelling is adopted. The turbulence model is the Shear Stress Transport (SST).

2. Governing Equations, Turbulence Model and Numerical Methodology

The governing equations in Cartesian coordinates of the analysed flow are the averaged continuity equation and the momentum equation shown below [15]

$$\frac{\partial}{\partial x_j}\left(\overline{u_j}\right)=0; \tag{1}$$

$$\frac{\partial}{\partial t}\rho\left(\overline{u_j}\right)+\frac{\partial}{\partial x_k}\rho\left(\overline{u_j}\,\overline{u_k}\right)=-\frac{\partial\overline{p}}{\partial x_i}+\frac{\partial\overline{\tau_{ij}}}{\partial x_i}+\frac{\partial}{\partial x_k}+\rho\left(\nu_t\left(\frac{\partial\overline{u_j}}{\partial u_k}+\frac{\partial\overline{u_k}}{\partial u_j}\right)\right) \tag{2}$$

where u_j and x_j are the velocity and spatial components, ρ the density, t the time, p is the pressure, τ_{ij} the viscous stress tensor, and ν_t is the eddy viscosity, that will be modelled inside of a closure context in first order, using the Shear Stress Tensor (SST) model.

The SST model was created originally by Menter et al. [16]. It possesses two groups of transport equations that depend on the spatial region. If the analysis is close to the wall, it uses the κ-ε formulation, if it does not use κ-ω formulation [17]. In the following it is shown the additional transport equations of this model:

$$\rho\frac{\partial k}{\partial t}+\rho\overline{u_j}\frac{\partial k}{\partial x_j}=\frac{\partial}{\partial x_j}\left(\left(\mu+\frac{\mu_t}{\sigma_{k1}}\right)\frac{\partial k}{\partial x_j}\right)+\widetilde{P}_k-\beta^*\rho\kappa\omega, \tag{3}$$

where

$$\widetilde{P}_k = \mu_t \frac{\partial u_i}{\partial x_j}\left(\frac{\partial u_i}{\partial x_j}+\frac{\partial u_j}{\partial x_i}\right) \rightarrow \widetilde{P}_k = \min\left(\widetilde{P}_k, 10\beta^* \rho\kappa\omega\right); \tag{4}$$

$$\rho\frac{\partial \omega}{\partial t}+\rho\overline{u_j}\frac{\partial \omega}{\partial x_j}=\frac{\partial}{\partial x_j}\left(\left(\mu+\sigma_{w1}\mu_t\right)\frac{\partial \omega}{\partial x_j}\right)+\alpha_1\rho S^2-\beta_1\upsilon\omega^2+ 2\left(1-F_1\right)\rho\sigma_{w2}\frac{1}{\omega}\frac{\partial \kappa}{\partial x_i}\frac{\partial \omega}{\partial x_i}, \tag{5}$$

where F_1, aims the determination of the constants in the model and also the variation of the transport equation of ω. Consequently, F_1 is defined as [16]:

$$F_1 = \tanh\left\{\left\{\min\left[\max\left(\frac{\sqrt{\kappa}}{\beta^*\omega y}, \frac{500\nu}{y^2\omega}\right), \frac{4\rho\sigma_{\omega 2}\kappa}{CD_{\kappa\omega}y^2}\right]\right\}^4\right\} \tag{6}$$

with

$$CD_{\kappa\omega} = \max\left(2\rho\sigma_{\omega 2}\frac{1}{\omega}\frac{\partial \kappa}{\partial x_i}\frac{\partial \kappa}{\partial x_i}, 10^{-10}\right), \tag{7}$$

and y is the distance of the sliding surface.

The other constants are all originated from the κ-ε and κ-ω models, with some fittings, being determined as: β^*=0.09, α_1=0.44, β_1=3/40, σ_{k1}=0.85, σ_{w1}=0.5, α_2=5/9, β_2=0.0828, σ_{k2} =1 and σ_{w2}=0.856 [15].

The turbulent viscosity is calculated by means of the following equation [15]:

$$\mu_t = \rho\frac{\alpha_1\kappa}{\max\left(\alpha_1\omega, \left(S_{ij}S_{ij}\right)^{1/2}F_2\right)}; \tag{8}$$

where $\left(S_{ij}S_{ij}\right)^{1/2}$ is an invariant measure of the rate of the strain tensor and F_2 is one of the combination equation determined by Eq. (9) having the aim to model the change in the turbulent viscosity formulation, depending on the flow region in analysis.

$$F_2 = \tanh\left\{\left[\max\left(\frac{2\sqrt{\kappa}}{\beta^*\omega y}, \frac{500\nu}{y^2\omega}\right)^2\right]\right\}. \tag{9}$$

The software used in the present work, the CFX 14, uses the method of the finite volumes. We use the unstructured mesh and for to achieve good performance in the analysis of boundary layer, the discretisation of the region near the wall is made dividing into several layers. The test section that comprises the computational domain is shown in Fig. 1. In this figure it is shown the inlet, upstream of the swirl, the own swirl, and its position in the flow, the diffuser with its total angle, and the exit section, downstream of the diffuser.

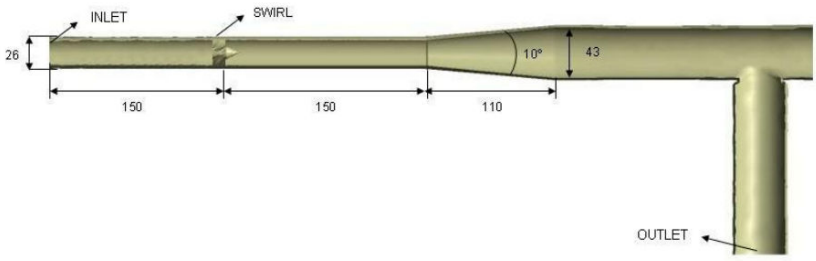

Fig. 1. Test Section of a Diffuser of Semi-angle of 5°, Equivalent to Total Angle of 10º (Dimensions in mm).

The diffusers used were 5° and 10°of the semi-angle. The boundary conditions utilized in the simulation consist in impose the same flow (next topic) rate in the entrance and in the exit of the test section used in the experimental measurements. It uses no slip condition on the walls.

3. Experimental Apparatus

In this work two diffuser geometries, one with semi-angle of 5° and the other with semi-angle of 10° are tested. Water flows in the diffuser in a closed circuit. The water flow rate in the test section is controlled by a frequency inverter, coupled to the motor of the centrifugal pump. The flow rate is measured by a rotameter. A water reservoir of 0.3 m^3, open to the atmosphere, feeds the test section and also receives the returning water. The experimental apparatus and the diffusers can be seen in Fig. 2.

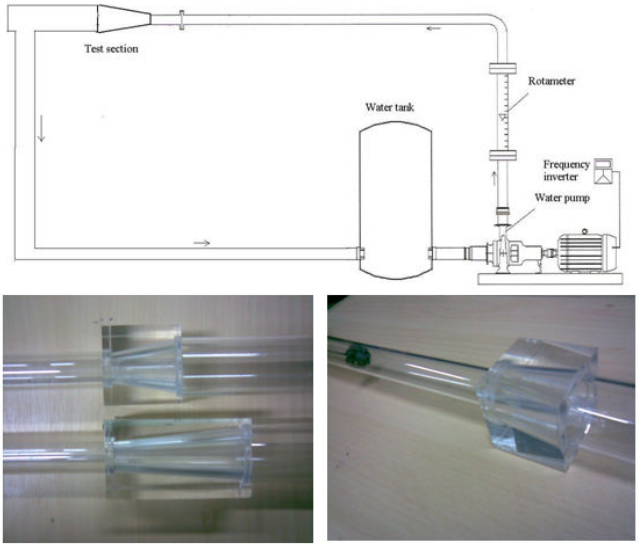

Fig. 2. The Experimental Setup (Top) and Acrylic Diffusers Used (Below).

The particles for Particle Image Velocimetry (PIV) are inserted in the water tank, in appropriate concentration and circulate with the water. Longitudinal measurements in the diffusers as well as transversal measurements in the test sections are accomplished. In each two-dimensional PIV measurements two orthogonal velocity components are obtained. For the measurement in a longitudinal plan of the diffuser a laser light sheet illuminates the test section horizontally, and the digital camera is placed with its axis in the vertical direction. For the measurement of components of speed in a transversal flow, the light sheet illuminates a vertical cross section and the digital camera now has its axis in the same direction of the diffuser axis. The light sheet is obtained with the aid of a cylindrical lens, coupled at the exit of the laser cavities. In the PIV system, utilized in this work, two pulsed laser cavities type Nyodim-YAG, with wavelength of 532 nm (green colour) and maximum frequency per cavity equal to 15 Hz operates in a synchronized way with the digital camera. This synchronization is made with a time hub. Figure 3 shows the configuration used for PIV.

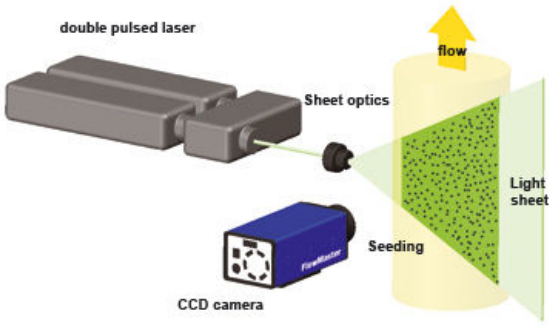

Fig. 3. Configuration Used for the PIV.

Appropriate software is responsible for the command, control, image acquisition and processing of the whole PIV process. This equipment is produced by IDT – Systems. In the present work, the acquisition frequency is set in 6 Hz and a group of 200 image-pairs were used for obtaining two mean velocities of the flows. Instantaneous flow characteristics are also obtained. In the PIV process, each image covering an area of 60 mm x 60 mm is subdivided in a group of 75 x 75 interrogation areas and, for each interrogation area, a velocity vector is associated. The calibration of the experiment and more details of the PIV can be found in Caldeira-Pires et al. [18].

4. Results and Discussions

This topic will be shown the results obtained in the comparison of numerical simulations and experimental.

Figure 4 presents the three-dimensional simulated flow result in a split way, between the swirler and the diffuser, and also inside the own diffuser, to facilitate the visualization. This simulation shows a typical turbulent flow that, when

passing through the swirler starts to present a swirling flow, rotating in a clockwise movement. The legend shows the intensity of the velocity vector.

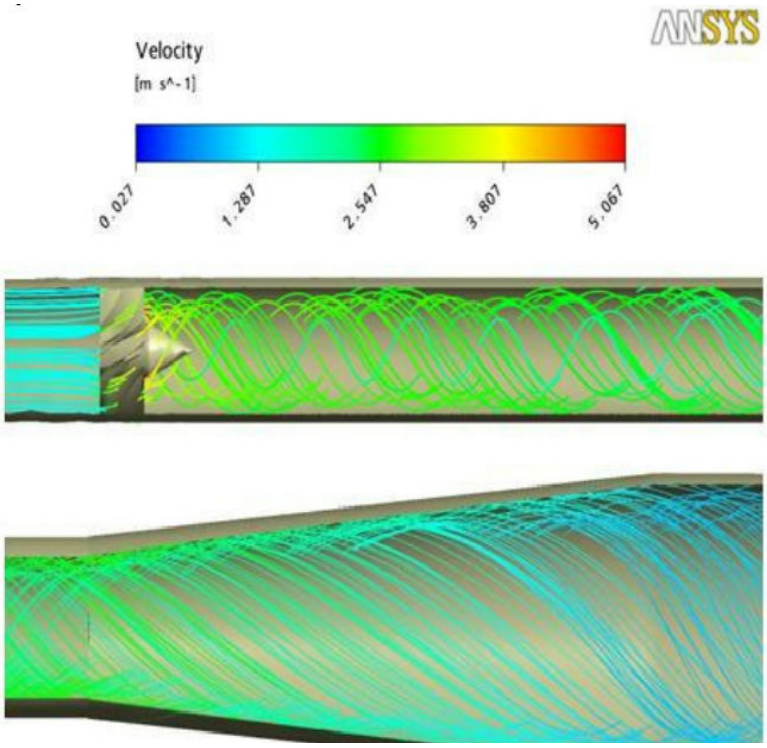

Fig. 4. Tridimensional Swirling Flow between the Swirl and the 10° Diffuser, and also Inside the Diffuser.

Figures 5 and 6 present experimental PIV results in the two cross sections between the swirler and the diffuser and also in the own diffuser with semi-angle of 10º. In the experiment the water flow rate was set in 40 liters per minute and the swirler was installed at 200 mm of the diffuser entrance. It was chosen, in this case, cross sections at four different longitudinal positions, to show the results obtained from the experimental measurements, which are, at 80 mm of the swirler, 140 mm of the swirler, 30 mm from the diffuser entrance, and also at 50 mm of the diffuser entrance. The flow characteristic is symmetrical in relation to the axial axis, then, the velocity components of horizontal and vertical have approximately equal values. The authors chose to use Cartesian coordinates and to show only the horizontal component of velocity, in m/s.

The flow enters in the diffuser, as shown in the measurements in diffuser cross sections in the Fig. 6, with the maximum velocity component of the secondary flow is of the order of 1m/s at a distance of 30 mm of the diffuser entrance, decreasing for about 0.7 m/s at a distance of 50 mm of its entrance. Figures 7 and 8 show the results of the numerical simulation in the respective cross sections already shown for the experimental results, in other words, between the swirler and the diffuser and in the cross sections of the own diffuser.

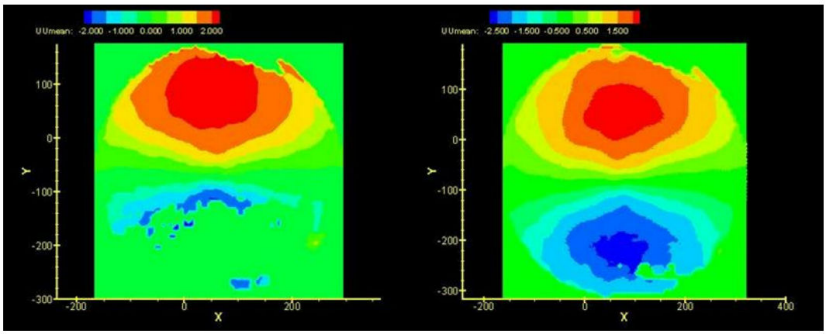

Fig. 5. Horizontal Velocity Components for the De 10º Diffuser, on the Cross Sections at 80 mm and 140 mm from the Swirler Exit.

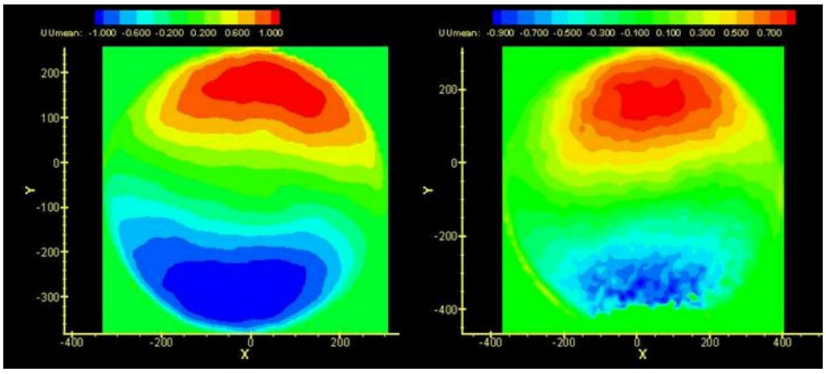

Fig. 6. Horizontal Velocity Components inside the 10º Diffuser, on the Cross Sections at 30 mm and 80 mm from the Diffuser Entrance.

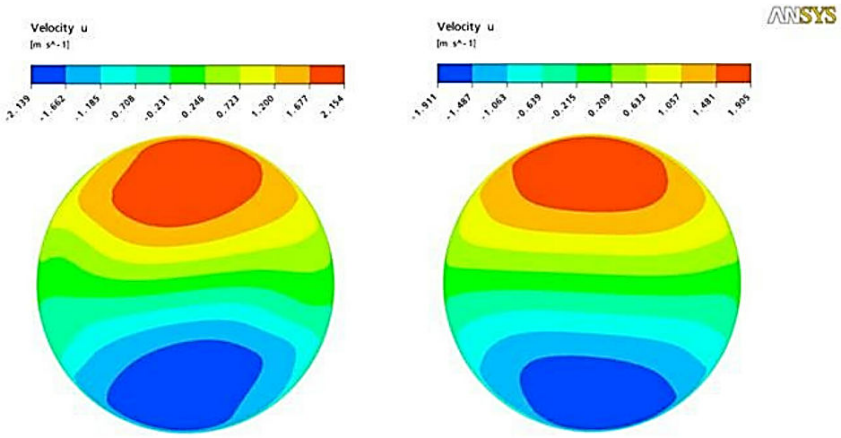

Fig. 7. Horizontal Velocity Components for the De 10º Diffuser, on the Cross Sections at 80 mm and 140 mm from the Swirler.

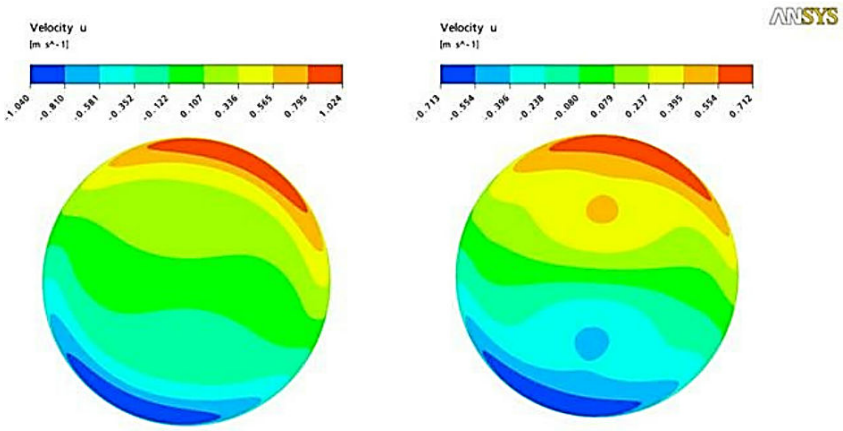

Fig. 8. Horizontal Velocity Components inside the 10º Diffuser, at Cross Sections at 80 mm and 140 mm from its Entrance.

The simulated results, downstream of the swirler, on the cross sections at 80 mm and 140 mm, also present a swirling flow, with maximum horizontal speed of the order of 2.15 m/s and 1.9 m/s, respectively. Inside the diffuser, in the cross sections at 30 mm and 50 mm of its entrance, the horizontal maximum speed is of the order of 1.0 m/s and 0.7 m/s. The experimental and numerical results present very close values, where the numerical analysis overestimated the results.

Figure 9 presents the longitudinal flow inside the diffuser of semi-angle equal to 10°. The experimental and numerical results show a diffuser operating with a large central recirculation zone. This recirculation occurs by elevated angle of the diffuser. The numerical results present values of axial speed in this recirculation region with larger intensity than those obtained by the experiments. It is believed that this discrepancy is due to the turbulence modelling. The more intense axial speeds occur in the entrance of the diffuser, in the regions close to the wall. This is because of the recirculation of the flow in the entrance the diffuser [12].The maximum values of these measured axial speeds are of the order of 1.4 m/s, while those obtained by simulation show values of the order of 2.1 m/s. In the recirculation region the experimental data present maximum axial speeds of the order of -0.2 m/s, while in the simulation they are around -0.6 m/s, where again the numerical analysis has overestimated the results.

Figures 10 and 11 shows the experimental and numerical results in the diffuser of 5°, where the results refer to the positions of 90 mm and 120 mm downstream of the swirl. The swirl was installed, in this case, at 150 mm of the diffuser entrance. For 90 mm, the values of maximum horizontal speed very similar, equal to 2, both in the experimental and numerical analysis. For 120 mm of the swirler, the numerical results are larger than the experimental data, being 1.6, while the experiment was equal to 1. It is believed also that this discrepancy too is due to the turbulence modelling.

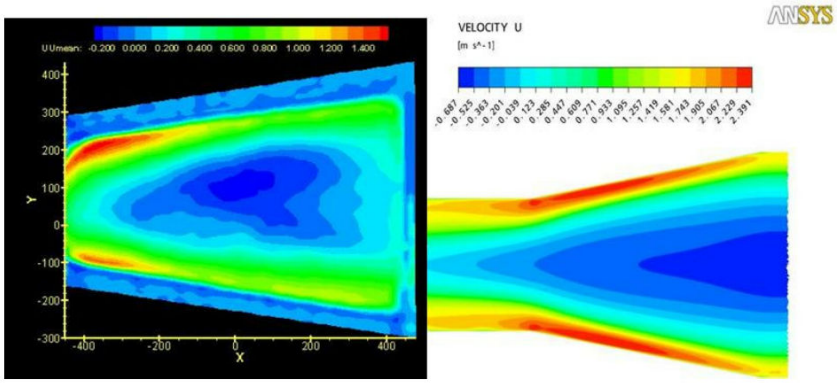

Fig. 9. Longitudinal Flow inside the 10º Diffuser.

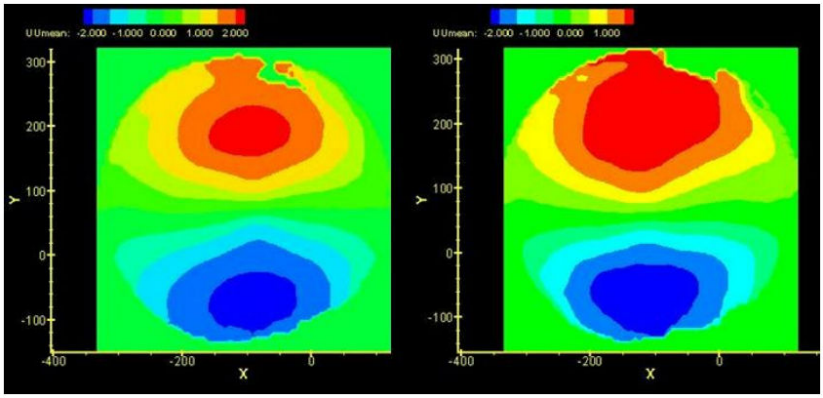

Fig. 10. Horizontal Velocity Components for the De 5º Diffuser, Cross Sections at 90 mm and 120 mm from the Swirler Exit.

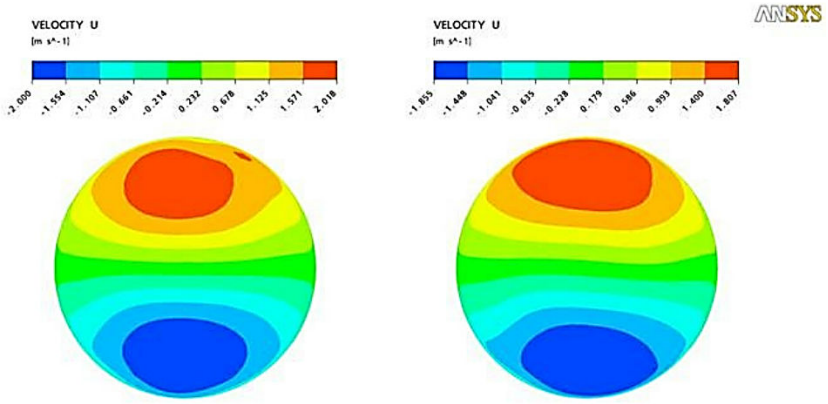

Fig. 11. Simulated Horizontal Velocity Components for the De 5º Diffuser, Cross Sections at 90 mm and 120 mm from the Swirler Exit.

Figure 12 presents the experimental and numerical longitudinal velocities results, for the diffuser of semi-angle equals 5º. The experimental results are presented in two images, since the PIV acquisition system only cover an image surface of 60 mm × 60 mm and the total length of this diffuser is equal to 110 mm. The superposition of these two PIV images is equal to 5 mm. Likely to the data found for the diffuser of semi-angle of 10^{o}, there is a large recirculation region dominating the diffuser flow. There is this recirculation because the flow enters rotating. If the inlet flow is normal in the diffuser entrance, these recirculation does not exist. The experimental data show axial recirculation speeds of the order of -0.2 m/s in this region, while the results of the numerical simulation present maximum values of the order of -0.5 m/s. The maximum axial positive speeds happen again in close regions of the diffuser wall, with experimental values of the order of 1.3 m/s and simulated data of the order of 2.15 m/s.

When analyzing the velocities longitudinal in diffusers, comparing the experimental results for the two semi-angles, it is noticed that the values are very close, with 1.4 m/s for the diffuser 10 ° and 1.3 for the diffuser 5°. The same is true when comparing the numerical simulations for the diffuser with 10º to obtain the speed of 2.3 m/s. For the diffuser with 5° the velocity is 2.1 m/s. So, it is noticed that for the semi-angles used, the values of the velocity are very close (experimental X experimental and numerical X numerical), showing that these semi-angles do not influence considerably the velocity field inside the diffuser.

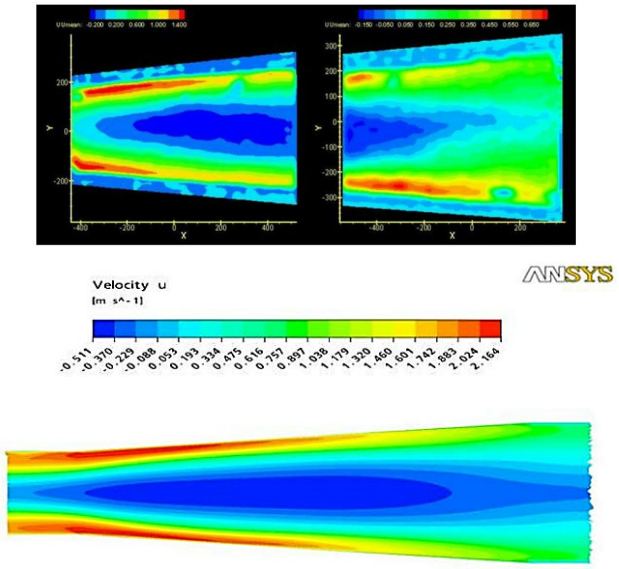

Fig. 12. Longitudinal Flow inside the Diffuser of Total Angle Equal to 5°.

5. Conclusion

The swirling flow in two different diffuser geometries were studied in the present work using Particle Image Velocimetry (PIV) and Numerical Simulation with CFX 14. The purpose is to compare the results obtained through horizontal velocity, also

analysing the recirculation, where the objective of finding quantitative results was reached. Data were reasonable, where, in general, numerical data over-assessed the results, however, it was evident that for best results, further research will be needed in the modelling of turbulence and the need to consider an Unsteady Reynolds Averaged Navier-Stokes (URANS) because the RANS methodology together with Shear Stress Tensor (SST) were unable to accurately predict the exact values of velocity and recirculation in the geometries studied.

References

1. Mulu, B.G.; Jonsson, P.P.; and Cervantes, M.J. (2012), Experimental investigation of a Kaplan draft tube – Part I: Best efficiency point. *Applied Energy*, 93, 695-706.
2. Wen, C.; Cao, X.; Yang, Y.; and Li, W. (2012). Numerical simulation of natural gas flows in diffusers for supersonic separators. *Energy*, 37(1), 195-200.
3. Bruce, A.R.; and Louis, P.R. (1962). Equilibrium between phases in converging-diverging nozzles. *Detonation and two-phase flow*, 6, 209-240.
4. Hac, C. (1983). Calculation of various diffuser flow with inlet swirl and inlet distortion effects. *American Institute of Aeronautics and Astronautics*, 21(8), 1127-1133.
5. Azad, R.S. (1996). Turbulent flow in a conical diffuser: A review. *Experimental Thermal and Fluid Science*, 13(4), 318-337.
6. Ishizaka, K.; Wakazono, S.; Yuri, M.; and Takahasdi, R. (2003). CFD studies of industrial gas turbine. *Proceedings of the International Gas Turbine Congress*.
7. Clausen, P.D.; Kish, S.G.; and Wood, D.H. (1993). Measurement of a swirling turbulent boundary layer developing in a conical diffuser. *Experimental Thermal and Fluid Science*, 6(1), 39-48.
8. Edwards, R.J.; Janbunathan, K.; Button, B.L.; and Rhine, J.M. (1993). A comparison of two swirl. *Measurement Techniques, Experimental Thermal and Fluid Science*, 6(1), 5-14.
9. Japikse, D. (2002). Correlation of annular diffuser performance with geometry, swirl, and blockage. *Proceedings of the 11th NASA/OSU Thermal and Fluid Analysis Workshop,* 107-118.
10. Iaccarino, G. (2000). Prediction of the turbulent flow in a diffuser with commercial CFD codes. *Annual Research Briefs*, 271-279.
11. Coelho, J.G. (2006). *Estudo Numérico de Tubos de Sucção de Turbinas Hidráulicas Tipo Bulbo*. Dissertação de Mestrado. Universidade de Brasília.
12. Coelho, J.G.; and Brasil, A.C.P.J. (2006). Simulação Numérica da Influência do Swirl em Difusores, *11th Brazilian Congress of Thermal Sciences and Engineering*.
13. Blevins, R.D. (1984). *Applied fluid dynamics handbook*, Van Nostrand Reinhold Company, England, 145.

14. Armfis, S.W.; Cho, N.; and Fletcher, A.J. (1990), Prediction of turbulence quantities for swirling flow in conical diffusers, *American Institute of Aeronautics and Astronautics,* 23(3), 453-460.
15. Kovalec, N.H. (1949). *Hydroturbine Design and Construction*, Israel Program for Scientific Translation, Jerusalem.
16. Menter, F.R. (1994). Two-equation eddy-viscosity turbulence models for engineering applications. *AIAA Journal*, 32, 1598-1605.
17. Menter, F. R.; Kuntz, M.; and Langtry, R. (2003). Ten years of industrial experience with the SST turbulence model. *Turbulence, Heat and Mass Transfer* 4.
18. Caldeira-Pires, A.; Souza, A.J.; and Neiva, Q.R. (2007). Swirling flow analysis using PIV. *Proceedings of COBEM 2007*.